Multiwalled Boron Nitride Nanotubes: Growth, Properties, and Applications

Jiesheng Wang, Chee Huei Lee, Yoshio Bando, Dmitri Golberg and Yoke Khin Yap

Abstract This chapter provides a comprehensive review on the current research status of boron nitride nanotubes (BNNTs), especially the multiwalled nanostructures. Experimental and theoretical aspects of the properties, synthesis, and characterization of BNNTs, as well as their potential mechanical, electronic, chemical, and biological applications are compiled here.

1 Introduction

Boron nitride nanotubes (BNNTs) were theoretically predicted in 1994 [1, 2] and experimentally realized in the following year [3]. As described in the previous chapter, BNNTs are structurally similar to carbon nanotubes (CNTs). Thus, BNNTs exhibit extraordinary mechanical properties like CNTs [4–6]. Despite these similarities, BNNTs are different from CNTs in other aspects. BNNTs possess nearly uniform electronic properties that are not sensitive to their diameters and chiralities [1, 2]. Theoretically, their band gaps (~5 eV) are tunable and can even be eliminated by transverse electric fields through the giant DC Stark effect [7–9]. Golberg et al. have shown that BNNTs are having high oxidation resistance [10], which was later confirmed by others [11, 12]. Recent result indicates that purified BNNTs are resist to oxidation up to 1,100°C [12]. In addition, BNNTs are predicted to have piezoelectricity [13, 14] and are applicable for room-temperature hydrogen storage [15]. Junctions of CNTs and BNNTs [16] are expected to produce itinerant ferromagnetism and spin polarization [17]. Obviously, these properties make BNNTs very attractive for innovative applications in various branches of science and technology.

J. Wang, C.H. Lee and Y.K. Yap (✉)
Department of Physics, Michigan Technological University, 118 Fisher Hall,
1400 Townsend Drive, Houghton, MI 49931, USA
e-mail: ykyap@mtu.edu

Y. Bando and D. Golberg
World Premier International Center for Materials Nanoarchitectonics (MANA),
National Institute for Materials Science, Namiki 1-1, Tsukuba, Ibaraki 305-0044, JAPAN

However, the growth of BNNTs is challenging. In the last 10 years, BNNTs were grown by arc discharge [3, 18, 19], laser ablation [20, 21], substitution reactions from CNT$_s$ [22], ball-milling [23], chemical vapor deposition (CVD) [24], boron oxide CVD (BOCVD)/floating zone method [25, 26], etc. These BNNTs contain impurities including amorphous boron nitride (a-BN) powders and other solid-state by-products. It is also challenging to use these techniques to directly grow BNNTs on substrates. Recently, Yap et al. have acquired for the first time the growth of *pure* BNNTs directly on substrates at significantly low temperature (~600°C) [27]. On the other hand, recent advancement in BOCVD has enabled mass production of BNNTs and the demonstration of a series of potential applications of BNNTs. In view of all these progresses, this chapter is devoted to highlight properties, synthesis, and potential applications of BNNTs.

The remaining of this chapter will provide more description in particular multi-walled (MW) BNNTs. In Sect. 2 of this chapter, various properties of MW-BNNTs will be discussed. Some of the prospective growth techniques of MW-BNNTs are highlighted in Sect. 3. Section 4 describes potential applications of BNNTs for polymer composites, electronic devices, and molecular biological and chemical applications. Readers are encouraged to read more about the experimental aspects of single-wall BNNTs in Chap. 3 and the related theory in Chaps. 4 and 5.

2 Properties of BNNTs

2.1 Mechanical Properties

The elastic properties of an individual MW-BNNT have been carefully studied by thermal vibration method [28]. The axial Young's modulus for a MW-BNNT with this method was found to be 1.18 TPa, which surpasses that of all other known insulating nanostructures. This experimental value is consistent with theoretical calculations performed by tight-binding (TB) methods [29]. However, recent in situ bending test on individual MW-BNNTs under transmission electron microscopy (TEM) demonstrated lower values of 0.5–0.6 TPa [30]. The lower detected modulus was probably due to the presence of polygonal cross-section morphology of MW-BNNTs. On the other hand, the BNNT could recover amazingly after relieving the load for severe bending.

2.2 Thermal Properties

High-density nanoelectronic devices are expected to generate tremendous heat radiation. This has initiated a strong demand of nanomaterials with good thermal conductivity. Various calculation approaches, including tight-binding method, density functional theory, and valence shell model, have been performed in order to address
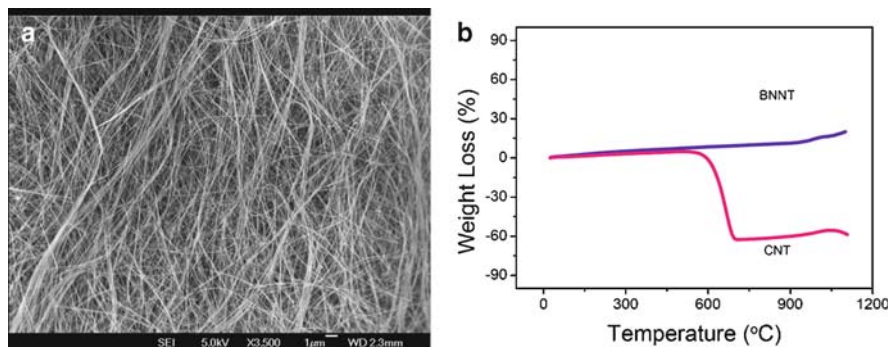
Fig. 1 (**a**) Scanning electron microscopy image of purified boron nitride nanotubes grown at 1,500°C, and (**b**) Comparative thermogravimetric analysis curves of BNNTs and CNTs (reprinted from [12]. © American Chemical Society)

the thermal properties of BNNTs [31–33]. It was shown that BNNTs would have a larger low-temperature thermal conductivity [34] than CNTs given that BNNTs have the same phonon mean free path as CNTs. However, it was demonstrated by experiment that pure and collapsed BNNTs are estimated to have thermal conductivity, κ, of ~18 and ~46 W/mK, respectively [35]. These values are far lower than the conductivity of the sintered bulk hexagonal BN particles at room temperature (>200 W/mK).

Another noteworthy thermal property of BNNTs is their high resistance to oxidation. A systematic study was first performed by Golberg et al. [10] and 3 years later by Chen et al. [11]. Recent study with purified MW-BNNTs grown at 1,500°C (Fig. 1a) indicated that BNNTs were stable at 1,100°C in air (Fig. 1b) [12]. The oxidation temperature for CNTs was ~500°C under similar thermogravimetric analysis.

2.3 Electronic Properties

BNNTs are theoretically predicted to have merely uniform electronic properties that are hardly modified by their chiralities or diameters [1, 2]. Moreover, zigzag BNNTs with chirality $(n, 0)$ are expected to have direct band gap. On the other hand, armchair BNNTs with chiral vectors (n, n) will have indirect band gap [19]. Because of their large band gap of ~5 eV, experiments using SW-BNNTs as the conduction channel for field-effect transistors (FETs) showed that BNNTs allowed transport through only the valence band [36].

Another important feature about the band gaps of BNNTs is that they are tunable by doping with carbon [37], radial deformation [38], or by applying a transverse electric field across the BNNTs – the so-called giant Stark effect [7–9]. Theoretical band structure calculations suggested that BNNTs can either be *p*-type or *n*-type semiconductors by controlling the composition of carbon into BNNTs. Carbon

impurities on the boron sites result in electron carriers while on the nitrogen sites result in hole carriers [37]. On the other hand, the band-gap modification by radial deformation in BNNTs was predicted through first-principles pseudopotential density-functional calculations. In zigzag BN nanotubes, radial deformations due to transverse pressures of about 10 GPa decrease the direct band gap of BNNTs from 5 to 2 eV, allowing for optical applications in the visible range. However, the band gaps of armchair BNNTs are found to be insensitive to radial deformations. Finally, theory indicates that the band gap of BNNTs can be reduced and even completely removed by the application of transverse electric fields. Experimentally, the giant Stark effect has been observed when applying a scanning tunneling microscopy (STM) tip to impose a local transverse electric field onto BNNTs and simultaneously probing the electronic properties [9].

2.4 Piezoelectric Properties

Another appealing property of BNNTs is piezoelectricity. This phenomenon theoretically originated from the deformation effect due to the rolling of the planar hexagonal BN networks to form tubular structures [13]. Nakhmanson et al. showed that BNNTs could be excellent piezoelectric systems [14]. As an example of calculations, piezoelectric constant for different zigzag BNNTs was found to increase along with the decrease of the radius of BNNTs [14]. It has been also proposed that a (5, 0) BNNT would have the largest piezoelectric constant for all investigated BNNTs.

Experimentally, Bai et al. have shown that under in situ elastic bending deformation at room temperature inside a 300-kV high-resolution transmission electron microscope, a normally electrically insulating MW-BNNT may transform to a semiconductor [39]. The semiconducting parameters of bent MW-BNNTs squeezed between two approaching gold contacts inside the pole piece of the microscope had been retrieved based on the experimentally recorded I–V curves. Remarkably, the nanotubes' electrical transport properties were found to be smoothly tuned from insulating to semiconducting through a bending deformation. Importantly, such unique transition was reversible. This could have been the first experimental sign suggestive of piezoelectric behavior in deformed BNNTs. Since BNNTs possess excellent mechanical properties, the detected deformation-driven tuning of BNNT electrical properties may have many interesting prospective applications in the nanoscale sensors, actuators, and advanced nanoelectromechanical systems (NEMS) with integrated electronic/optical functions.

2.5 Electron Field Emission Properties

Field emission properties of BNNTs have been tested by Cumings et al. using an in situ manipulation stage inside a TEM system [40]. The turn-on voltages for BNNTs were approximately twice higher than that for CNTs of similar geometries that

were measured with the same setup. The current densities were similar in both cases. In the Fowler-Nordheim plot for BNNTs, a single slope can be observed compared with the case of CNTs where the current often shows saturation at high electric fields or two distinct Fowler–Nordheim slopes are often observed. Besides, BNNTs showed more stable field emission with less noise. However, these results require further confirmation with high-purity BNNTs in the future.

2.6 Optical Properties

A local-density approximation (LDA) calculation has pointed out that optical band gap of BNNTs is independent of the chirality [41]. Another interesting point related to their optical properties is the photoelectric effect. According to Kral et al., unpolarized light can induce a shift current in BNNTs, with a direction along the tube axis [42]. These photoelectric effects can lead to new optoelectronic, optomechanical, and magnetic applications.

To understand polarizabilities of BNNTs, Kongsted et al. investigated the polarizability tensors for several types of single-wall BNNTs and compared with corresponding CNTs [43]. Their computations showed that BNNTs had smaller magnitudes of the polarizability tensor components than those of CNTs with the same geometry and number of atoms. Polarizability tensor of BNNTs is shown to depend on the tubule length, chiralities, light frequency, etc.

A comprehensive review on the vibrational and optical properties of BNNTs is compiled in Chap. 5 of this book.

3 Synthesis of BNNTs

As described, the synthesis of BNNTs is far more challenging than the growth of CNTs. Some of the growth techniques resembling those for the synthesis of CNTs were shown to work for the growth of BNNTs but some others required very specific growth system and procedures. The details of these approaches are compiled in this section.

3.1 Arc Discharge

The arc discharge method that first successfully grew BNNTs was similar to that for growing CNTs [3]. In the case of BNNTs, the anode was built by inserting a h-BN rod into a hollow tungsten electrode and the cathode was a rapidly cooled pure copper electrode. Arc discharge occurred between the tungsten and copper electrodes. The inserted h-BN rod was evaporated indirectly. After the arc discharge,

the gray product was deposited on the copper cathode, which contented some scattered single-wall BNNTs. Other successful attempts to grow BNNTs by arc discharge method were using hafnium diboride (HfB_2) electrodes [19] and arcing hexagonal boron nitride (h-BN) and tantalum in a nitrogen atmosphere [18].

3.2 Laser-Based Methods

Laser heating is one of the possible methods to synthesize BNNTs as demonstrated by Golberg et al. [44]. Single crystal c-BN specimens were laser heated in a diamond anvil cell under high nitrogen pressures. TEM and other characterization techniques confirmed the product to be BNNTs.

Another laser-based technique was oven-laser ablation method [20]. The target material was prepared by mixing high-purity h-BN and nanosized Ni and Co powders. The target was then placed inside a long quartz tube heated by a tube furnace. An excimer laser with a wavelength of 248 nm was focused on the target to initiate ablation. At optimum laser pulsed energy and oven temperature (1,200°C), the ablated laser plumes were carried by the flowing gas and collected on the water-cooled copper collector. BNNTs with diameters ranging from 1.5 to 8 nm were obtained together with other amorphous byproducts. Comparison of the structure of the BNNTs synthesized with different carrier gases revealed an interesting phenomenon. BNNTs obtained in inert argon and helium gases were dominated with single-wall BNNTs. When nitrogen was used as the carrier gas, the BNNTs were dominated with double-wall structures. No BNNTs with more than four walls were observed.

Recently, single-wall BNNTs can be produced in high crystalline quality by Loiseau et al. This technique involves the vaporization of a hexagonal BN target by a continuous wave CO_2 laser under a nitrogen flow at a pressure of 1 bar. Readers should refer to Chap. 3 for the details.

3.3 Substitution Reaction

Because of the nearly identical lattice structure between CNTs and BNNTs, the former were used as the templates to prepare BNNTs. This technique is called CNT-substituted reaction, where carbon atoms of CNTs are substituted by boron and nitrogen atoms [22] according to the reaction formula as follows:

$$B_2O_3 + 3C \text{ (CNTs)} + N_2 \rightarrow 2BN \text{ (BNNTs)} + 3CO$$
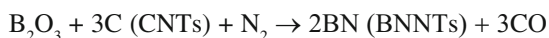
The reaction was performed in an induction-heating furnace. In brief, B_2O_3 powder was placed in an open sintered graphite crucible and then covered with CNTs.

The crucible was kept in a flowing nitrogen atmosphere at 1,500°C for half an hour. Followed by cooling, the starting black CNTs were found to turn into gray color. Different characterization techniques confirmed that BNNTs were grown but were mixed with carbon and other BN phases. To purify the product, oxidation treatment could start to oxidize carbon layers around 550°C and transform these mixed-phase nanotubes into pure BNNTs.

3.4 Ball-Milling Technique

Ball-milling is a technique that can produce BNNTs at high yield, but it has a disadvantage of low purity [11, 45]. As reported by Chen et al., the ball-milling system has four stainless steel milling vessels with each small vessel loaded with several grams of boron powder and four hardened steel balls. Then, they were filled with ammonia gas at a pressure of 300 kPa prior to milling. With this method, four large vessels could mill powder up to 1 kg. The mechanism behind was the transfer of large amount of mechanical energy into boron powder particles, leading to morphological, structural, and chemical changes. Followed by milling, an isothermal annealing was executed in a tube furnace at 1,200°C for 16 h under nitrogen gas flow. Finally, BNNTs were obtained by converting powder to tubules with the formation yield of 65–85% [45]. It is noted that most of these BNNTs appeared in bamboo-like structures.
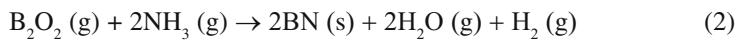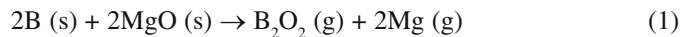
3.5 Catalytic CVD

Catalytic CVD (CCVD) is one of the most popular and successful techniques for the synthesis of CNTs and various nanowires. Lourie et al. described the growth of BNNTs by using borazine ($B_3N_3H_6$) as the precursor according to the chemical reaction as follows [24]:

$$3(NH_4)_2SO_4 + 6NaBH_4 \rightarrow 2B_3N_3H_6 + 3Na_2SO_4 + 18H_2$$
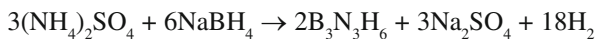
The growth was all successful in trials applying different catalysts such as Co, Ni, NiB, or Ni_2B. The NiB catalysts were found to be the most effective catalysts. The substrate coated with NiB or Ni_2B catalysts was placed in the center of the tube-furnace reactor that was heated to 1,000–1,100°C. These were then exposed to the $B_3N_3H_6$-containing carrier gas for half an hour. White deposits were observed on the substrate and were identified as MW-BNNTs. Recently, borazine was also used in conjunction with a floating nickelocene catalyst, resulting in the predominant formation of double-walled BNNTs [46].

Instead of using the dangerous borazine, Tang et al. have shown that boron oxide can be an effective precursor for the growth of BNNTs [12, 25, 26]. This was first demonstrated by applying the redox reaction between boron and oxides (SiO2;

Fe2O3) to generate boron oxide gas (B_2O_2) in the reaction area [25]. Therefore, when ammonia was introduced the growth of BNNTs was initiated with Fe_2O_3 as the possible catalyst as supported on alumina nanopowders. This approach was then improved by using a mixture of boron and magnesium oxide (with molar ratio of 1:1) located in a BN-made reaction tube. The system was heated to 1,300°C using an RF inducting furnace [26]. At this temperature, boron reacted with MgO to form B_2O_2, and Mg vapor acted as the floating zone catalyst. The vapors were argon-transported into a reaction chamber while a flow of ammonia was then introduced. BNNTs were synthesized by the simple reaction of B_2O_2 and ammonia. The chemical reactions are given by (1) and (2):

$$2B \text{ (s)} + 2MgO \text{ (s)} \rightarrow B_2O_2 \text{ (g)} + 2Mg \text{ (g)} \qquad (1)$$

$$B_2O_2 \text{ (g)} + 2NH_3 \text{ (g)} \rightarrow 2BN \text{ (s)} + 2H_2O \text{ (g)} + H_2 \text{ (g)} \qquad (2)$$

After fully evaporating the precursor mixture (1.55 g), 310 mg of white product could be collected from the BN wall of the chamber. The conversion rate from boron to boron nitride reached up to 40%. This effective technique is sometimes called BOCVD or floating zone CVD since both the precursors and catalyst are in vapor phase.

3.6 Other Synthesis Techniques

A brief description of other growth techniques for BNNTs is provided here.

3.6.1 Liquid Flow of FeB Nanoparticles

The synthesis of BNNTs and BN nanocages from the liquid flow of iron boride (FeB) nanoparticles was reported by the nitrogen plasma treatment of FeB nanoparticles [47]. Si wafers cast by FeB nanoparticles were introduced into a microwave plasma CVD system and then heated to 900°C during plasma treatment. Mixed gases of N_2 and H_2 were used as a gaseous precursor. After the plasma treatment, a whitish-gray product was formed, which included BNNTs. In addition to BNNTs (5–10-nm diameter), other nanostructures consisting of BN nanocages as well as BN hollow microspheres were present.

3.6.2 Electron Beam In Situ Deposition

Bengu et al. demonstrated the use of a low-energy electron cyclotron resonance (ECR) plasma to deposit SW-BNNTs [48]. Tungsten was used as a substrate after being prepared by specific polishing and cleaning. The growth chamber was kept at ultrahigh vacuum. During the growth, the clean substrates experienced a growth

temperature between 300 and 800°C and a pressure around 10^{-3} Pa under a negative DC bias of 300–600 V. To provide B source for BNNTs, a conventional electron-beam evaporation method was applied, while nitrogen ions provided N for BNNTs via a compact ECR source. As confirmed by in situ high-resolution TEM measurements, short SW-BNNTs were synthesized on tungsten substrates.

3.6.3 Plasma Jet Method

The reaction chamber for plasma jet method was implemented by a water-cooled plasma torch, target holder, and a powder collector, according to the report by Shimizu et al. [49]. A direct current (DC) arc plasma jet was formed at a power of 8 kW while the chamber pressure was maintained at 100 Torr. A BN sintered disk was used as a target and exposed to a plasma jet for 1 min, giving a temperature of 4,000 K on the sample, which was thus vaporized. BNNTs were found in a vaporized product.

3.7 Low-Temperature Growth of BNNTs

As a summary for previous methods, it is noted that most synthesis techniques for BNNTs required high growth temperatures and the products often contained impurities. Moreover, patterned growth at desired locations has not been achieved. Yap et al. showed that *pure* BNNTs could be directly grown on Si substrates at 600°C by a plasma-enhanced pulsed-laser deposition (PE-PLD) technique using Fe film catalyst [27]. Furthermore, these BNNTs were vertically aligned and could be extracted for device fabrication without purification.

Scanning electron microscopy (SEM) indicated the formation of bundled BNNTs (Fig. 2a–c). The growth locations of BNNTs were controllable due to the prepatterned Fe catalyst (Fig. 2d). TEM confirmed that the tubes were long and straight with a nominal diameter of 20–40 nm. The tips of these BNNTs were fully capped and did not contain catalyst particles, which suggested a base-growth mechanism.

The optimum growth of these BNNTs was obtained through an ideal combination of Fe film thickness, the laser energy density, and the substrate DC bias that induced film resputtering, etc. At a too high deposition rate, only BN films were grown on the substrates (Fig. 3a). The thickness of BN films gradually reduced with an increase in the substrate bias (Fig. 3b) until BNNTs started to grow, being balanced by a film deposition rate and a resputtering rate at a higher substrate bias (Fig. 3c). Under decent resputtering, the deposition of BN thin films was suppressed allowing the formation of BNNTs on Fe nanoparticles according to the vapor-liquid-solid (VLS) mechanism. The growth mechanism represents a phase-selective process between BN films and BNNTs. One of the functions of Fe particles was to capture the energetic BN growth species and confine the growth location. By means of scanning probe microscopy, the local density of electronic states (LDOS) of the BNNTs was measured. The band gaps estimated from the LDOS spectra were found to vary from 4.4 to 4.9 eV.
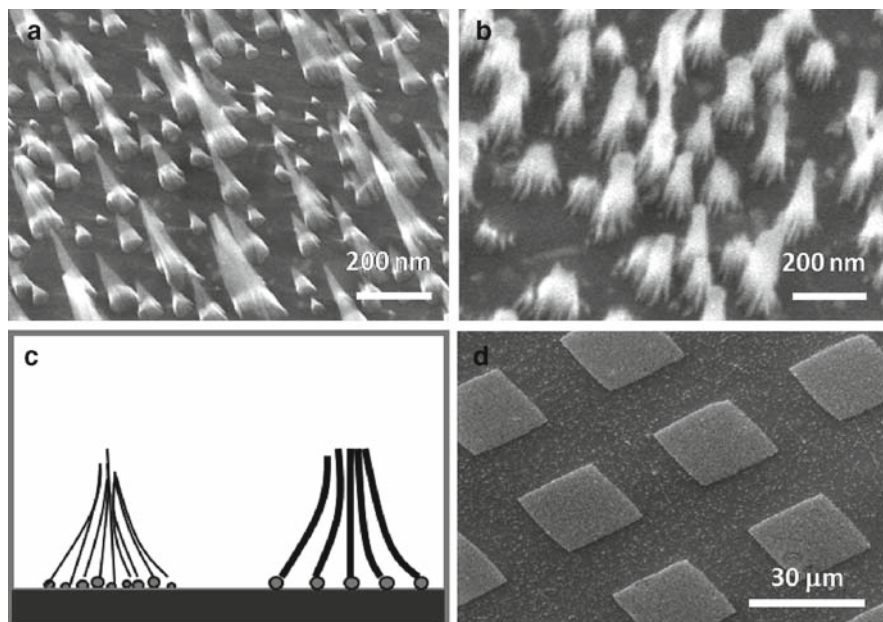
Fig. 2 SEM images of BNNT bundles with (**a**) smaller and (**b**) bigger diameters. Schematic of their corresponding bundling configurations is illustrated in (**c**). (**d**) Patterned growth of BNNTs (reprinted from [27]. © American Chemical Society)
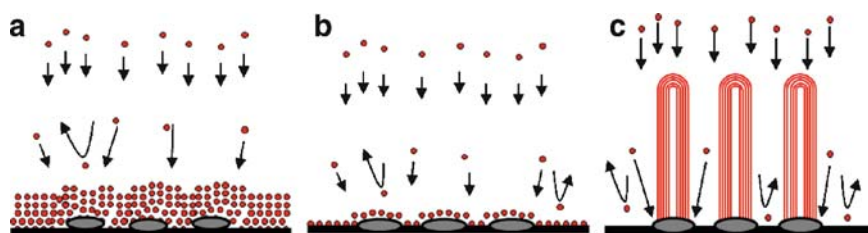

Fig. 3 Schematic of a phase-selective growth of BNNTs. (**a**) BN film deposition on Fe nanoparticles at low substrate biases. The film covers the catalysts due to a low resputtering rate of the growth species. (**b**) The growth rate starts to decrease as the substrate bias increases. (**c**) Resputtering becomes dominating and enables the growth of BNNTs (reprinted from [27]. © American Chemical Society)

3.8   Effective Growth of BNNTs in Horizontal Tube Furnaces

Recently, Yap et al. described a simple route that enables the growth of BNNTs in a conventional horizontal tube furnace [50]. This furnace consists of a quartz tube vacuum chamber, which is commonly used for the growth system of CNTs and

nanowires [51–57]. A mixture of B, MgO, and FeO (or Fe_2O_3) powders at a 2:1:1 molar ratio was used as a precursor (Fig. 4). These powders were placed in an alumina boat and loaded into a one-end closed quartz tube. The precursor materials were placed near the closed end of this quartz tube and located at the center of the vacuum chamber. Several Si substrates were placed on the top of the alumina boat. The chamber was evacuated to about ~30 mTorr before 200 sccm of NH_3 gas was introduced into the chamber. Subsequently, the precursors were heated up to 1,200°C for 1 h. Similar to the BOCVD technique using the induction heating method, at a high temperature, reactive B_2O_2 vapor was generated and reacted with NH_3 gas to form BNNTs. White-colored film was uniformly deposited over the whole area of the substrate.

As indicated by SEM, clean and long BNNTs were deposited on the Si substrates (Fig. 5). The tubular structures of these BNNTs can be easily observed with high-resolution SEM (Fig. 5b) and reconfirmed by TEM and electron energy loss spectroscopy (EELS) [50].

Typical Raman and Fourier transformed infrared (FTIR) spectroscopies of these BNNTs are shown in Fig. 6 [50]. A sharp Raman peak at ~1367 cm^{-1} can be detected (Fig. 6a), which corresponds to the E_{2g} in-plane vibration of the hexagonal
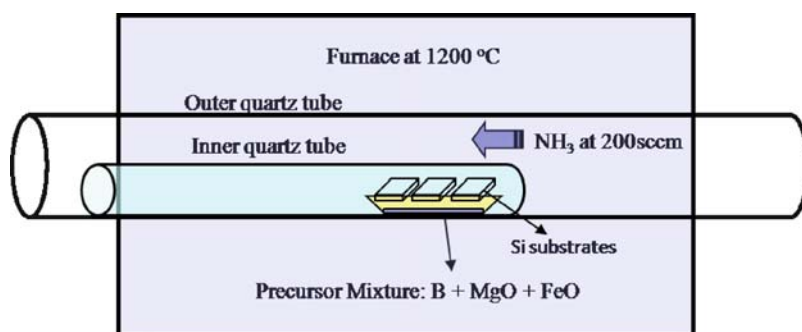

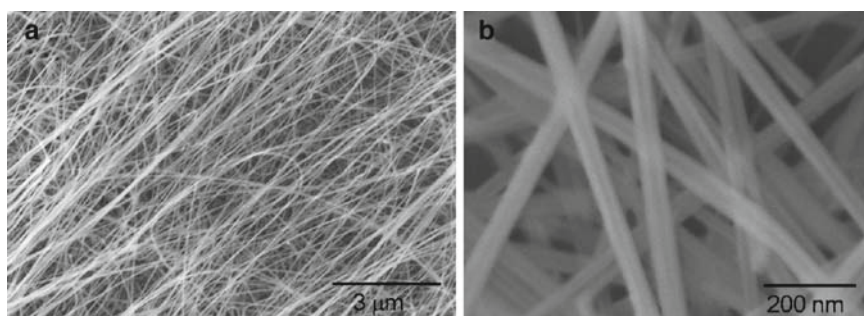**Fig. 4** Experimental setup for the growth of BNNTs by thermal CVD

Fig. 5 Scanning electron microscopy images of as-grown BNNTs at (**a**) low and (**b**) high resolution
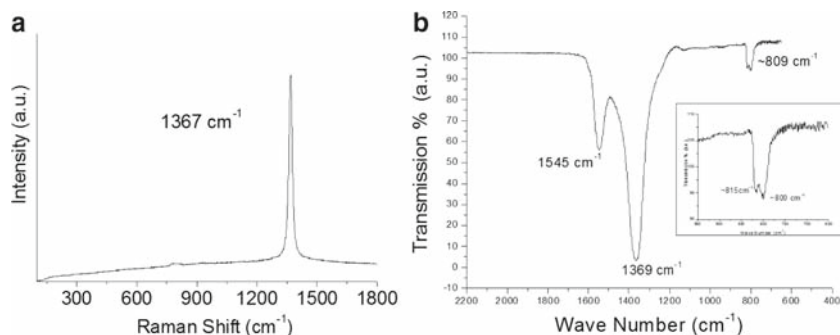
Fig. 6 Typical (**a**) Raman and (**b**) FTIR spectra of the as-grown BNNTs

BN (h-BN) networks. Three IR absorption frequency regimes can be obviously distinguished at ~809, ~1,369, and ~1545 cm^{-1} (Fig. 6b). The absorption bands at ~1,369 and ~1,545 cm^{-1} are attributed to the in-plane stretching modes of the h-BN networks. This has been explained by the zone-folding method, which considered BNNTs as the seamless cylindrical rolls of h-BN sheets [32]. The 1,369 cm^{-1} band is corresponding to the transverse optical (TO) mode of h-BN sheets that vibrates along the longitudinal (L) or tube axis of a BNNT. The absorption band at ~1,545 cm^{-1} is assigned to the stretching of the h-BN network along the tangential (T) directions of a BNNT. This stretching mode is corresponding to the longitudinal optical (LO) mode of the h-BN sheets, which is Raman inactive. It is also worth noting that this LO mode smears out for h-BN bulks or thin films, and only shows up when the tube curvature induces a strain on the h-BN networks. Thus, it is suggested that only highly crystalline BNNTs would show up this LO mode. In addition, it is noted that the T-mode vibration may shift between ~1,530 and ~1,545 cm^{-1}, from samples to samples. This is explained by the change of the average diameter of BNNTs in different samples, attributed to different curvatures of the h-BN sheets in BNNTs and thus the induced lattice strains along the tangential directions of the nanotubes. The absorption at ~809 cm^{-1} is associated to the out-of-plane radial buckling (R) mode where boron and nitrogen atoms are moving radially inward or outward. This interpretation is also identical to the out-of-plane bending mode of h-BN films [58, 59] with a small shift in wavenumber due to the strain developed on the tubular h-BN network in BNNTs. More interestingly, the authors observe a splitting of this R mode vibration at ~800 and ~815 cm^{-1}, as highlighted in the inset of Fig. 6b. Tentatively, it is thought that the splitting of the radial buckling vibration is related to the complex interaction of buckling vibration at different h-BN sheets that have different diameters and chiralities. However, the origin of this splitting will require further theoretical and experimental analysis in the future. More theoretical interpretation of these vibrational properties is available in Chap. 5.

UV–Visible absorption spectroscopy was also used to characterize these as-grown BNNTs. This was performed by a suspension of BNNTs in ethanol. Result indicates

that the optical band gap of these BNNTs is as large as ~5.9 eV [50]. The optical band gap detected here is larger than that reported for BNNTs (5.5 eV) grown by BOCVD in induction furnaces at higher growth temperatures [60]. The bandgap of our BNNTs is comparable to that of single-wall BNNTs [61] and hexagonal BN single crystals [62].

4 Potential Applications

Previous sections summarized experimental works particularly on the growth, properties, and characterization of BNNTs. The discussion on applications of BNNTs is rare in the literature due to present limitations and challenges of mass BNNT productions. However, recent publication especially those from Golberg et al. have indicated some potential applications of BNNTs. Some of these and others are summarized hereafter.

4.1 *Hydrogen Storage*

Hydrogen is regarded as an ideal and nonpolluting energy source that may become an alternative to replace current energy sources. However, hydrogen storage is among the obstacles toward real hydrogen energy technology. Nanomaterials can be more favorable than bulk counterparts with respect to molecular adsorptions due to large specific surface area. CNTs have been the potential materials for hydrogen storage due to their light mass density, high surface to volume ratio, and well-understood chemistry with hydrogen [63]. However, carbon-based materials have weak binding with hydrogen. This significantly restricts possible improvements. Also, experimental results from different groups have not been consistent, especially in regard to single-walled CNTs (SWCNTs) [64]. One possible reason might be due to the fact that SWCNTs can be either semiconducting or metallic, depending upon their diameters and chiralities, and thus have different electronic interactions with guest H_2 molecules and/or H atoms.

BNNTs are always semiconducting with a wide bandgap that is almost independent of the tube diameter and chirality. Moreover, the ionic character of B–N bonds may induce extra dipole moments favorable for stronger adsorption of hydrogen. The binding and diffusion energies of adsorbed hydrogen have recently been computed [65], and BNNTs were found to be suitable for room-temperature hydrogen storage. Also, diffusion through the active sites makes hydrogen penetration toward the inner BNNT surface possible and increases the storage capacity.

On the other hand, metal-doped BNNTs, as investigated by Wu et al., might be even better for hydrogen storage [63], because the presence of defects could enhance the adsorption of hydrogen atoms on BNNTs and reduce the dissociation barrier of the hydrogen molecule on their walls. Baierle et al. also claimed that moderate

substitutional doping in materials with ionic-like bonding, such as carbon-doped BNNTs, could enhance the binding energies of hydrogen, making them optimal for storage [66]. In experiments, Ma et al. showed that MW-BNNTs can absorb 1.8–2.6 wt% hydrogen under ~10 MPa at room temperature [67].

4.2 Functionlization

Tremendous research efforts have been made toward chemical functionalization of conventional CNTs since such materials show high potential in many fields of science and technology. It is an essential process to tailor properties of CNTs and make use of them in devices. Some of the motivations include enhancement of CNTs' solubility in solvents, prevention of bundling for better dispersion, production of CNTs composites and biologically compatible CNTs, etc. [68–72]. In particular, the covalent bonding of organic molecules to CNTs may provide a very interesting pathway to new applications in material science, chemistry, and medicine [73–81].

Because of the similarities in geometry it has been proposed that engineering of properties of BNNTs can be carried out along the same way as that of CNTs. Furthermore, a relatively wide band gap of BNNTs restricts their applications primarily to dielectric ones. Thus, it is desirable to control the band structure of BNNTs in order to suit different kinds of applications. The general pathways of functionalization of BNNTs include noncovalent bonding via π–π interactions between polymers, covalent attachments of molecules on BNNTs, and doping of BNNTs with exotic atoms.

Several pioneering works on functionalization of BNNTs were reported on covering BNNTs with semiconducting SnO_2 nanoparticles 1–5 nm in size [82, 83]. In fact, the work on functionalization of BNNTs has been hindered due to the challenges of producing pure BNNTs with a high yield. Recently, a significant breakthrough of producing grams of BNNT has been reported by Zhi et al. [84]. Soon after this, intensive functionalization works have been conducted by the same authors.

4.2.1 BNNT Composites for Mechanical Applications

Functionalization of BNNTs can be achieved through noncovalent interactions, i.e., wrapping BNNTs with a polymer. Because of the sp^2 hybridized h-BN network, most polymers with a long chain made of benzene rings can interact with the side walls of BNNTs through π–π stacking interactions. It had been shown that functionalized BNNTs were perfectly dissolved in many organic solvents [12, 85]. For example, the PmPV-wrapped BNNTs were fully soluble in chloroform, N,N-dimethylacetamide, and tetrahydrofuran, but insoluble in water and ethanol. Based on this particular interaction with BNNTs, the functionalization can be implemented to purify BNNTs from big particles and other impurities [86]. Furthermore, it was found that the composites of BNNTs with PmPV possess modified
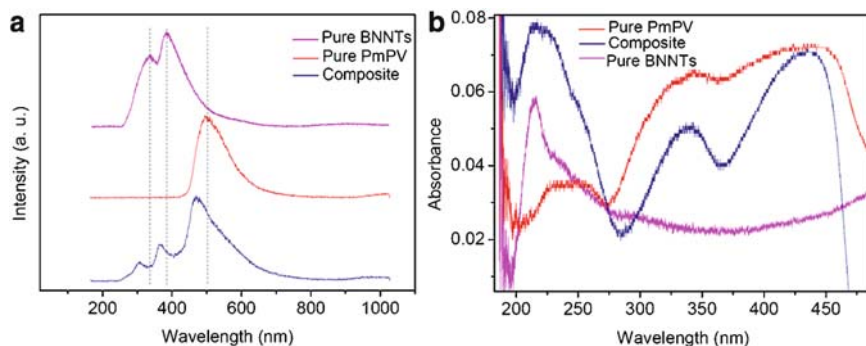
Fig. 7 (**a**) Comparative CL spectra and (**b**) UV−vis absorption spectra of pure BNNTs, pure PmPV, and a composite made of them (courtesy of C. Y. Zhi; reprinted from [12]. © American Chemical Society)

luminescence and absorption properties (Fig. 7), which were different from that of pure PmPV, due to the noncovalent interactions under polymer wrapping [12]. From TEM imaging (Fig. 8a), a layer of polymer (PmPV) can be clearly distinguished from a well-crystallized BNNT's side wall. The functionalized BNNTs are well dispersed on TEM grids as shown in the inset. Because of the remarkable mechanical properties of BNNTs, mixing BNNTs with a polymer may strengthen the polymer matrix for mechanical and reinforcement applications. As shown in Fig. 8b, functionalized BNNTs can be dissolved well in organic solvent while nonfunctionalized BNNTs will be precipitated. These functionalized BNNTs can be used for preparing transparent polystyrene (PS) composite film with 1 and 3 wt% of BNNTs as shown in Fig. 8c.

4.2.2 Bandgap Tuning for Electronic and Chemical Applications

The bandgap of BNNTs can also be modified by attaching molecules on the side walls covalently [87]. Covalent functionalization on the side wall of BNNTs had been performed by synthesizing stearol chloride-functionalized BNNTs through covalent interaction of –COCl groups with amino groups on the tube walls [88]. This particular work was based on the assumption that some of the amino groups remained on side walls of BNNTs during the synthesis process. Theoretical modeling after geometrical relaxation was performed (Fig. 9). It can be seen that a local distortion occurs near the adsorption site, which can be understood by the local sp^3 rehybridization of a N atom at the absorption site. From the band structure calculations, the HOMO–LUMO (highest occupied molecular orbital and lowest unoccupied molecular orbital) gaps decrease dramatically after functionalization due to new bands introduced into the gap (Fig. 10), which indicates that a charge transfer may take place and functional groups may have a dopant effect on BNNTs. The experimental evidence reveals that the functional groups binding on the side
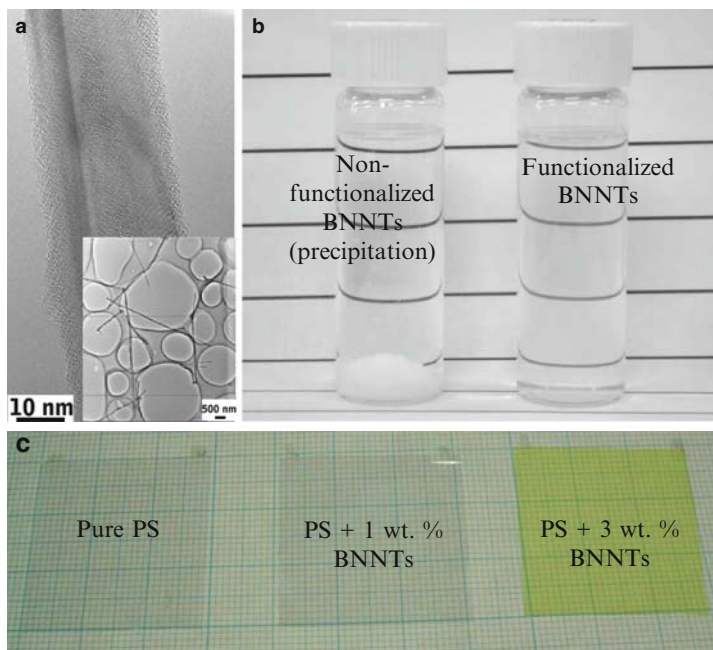
Fig. 8 (**a**) HRTEM image of a BNNT coated with PmPV (inset shows the well-dispersed BNNTs on a TEM grid), (**b**) images of two vials containing BNNTs in chloroform; note that the vial on the left shows BNNT precipitation at the bottom because the tubes were not functionalized with a polymer and are not soluble, whereas the vial on the right does not reveal precipitation because of preliminary BNNT functionalization with polystyrene (PS) or poly(methyl methacrylate) (PMMA), (**c**) composite films of PS with BNNTs after adding 1 or 3 wt% multiwalled BNNTs; note that the films are still transparent (courtesy of C. Y. Zhi)
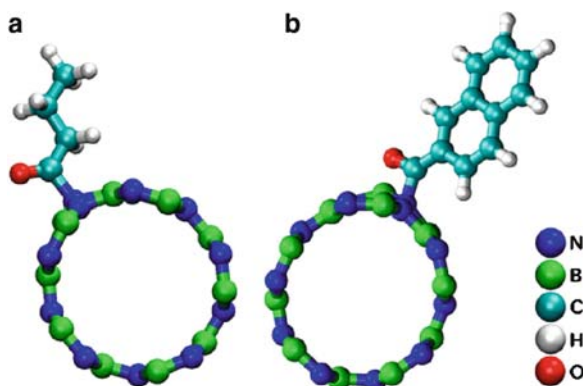
Fig. 9 The optimized structure of (**a**) $CH_3(CH_2)_2CO-BNNT$ and (**b**) $C_{10}H_7CO-BNNT$ (courtesy of C. Y. Zhi; reprinted from [87]. © American Physical Society)
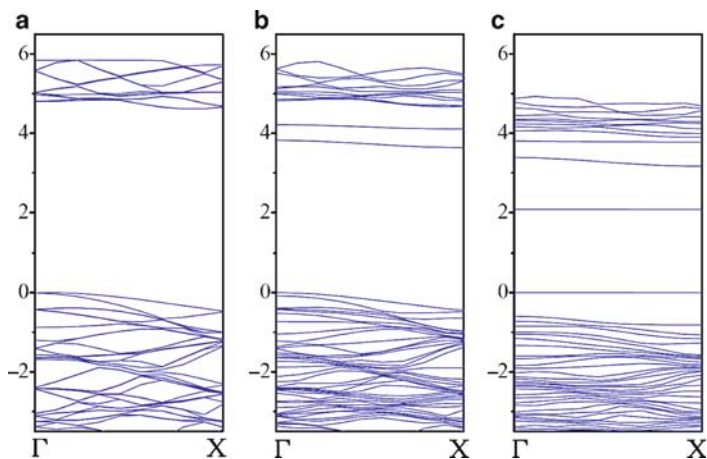
Fig. 10 Calculated bank structure of (**a**) a (5, 5) BNNT, (**b**) $CH_3(CH_2)_2CO$-BNNT, and (**c**) $C_{10}H_7CO$-BNNT (courtesy of C. Y. Zhi; reprinted from [87]. © American Physical Society)

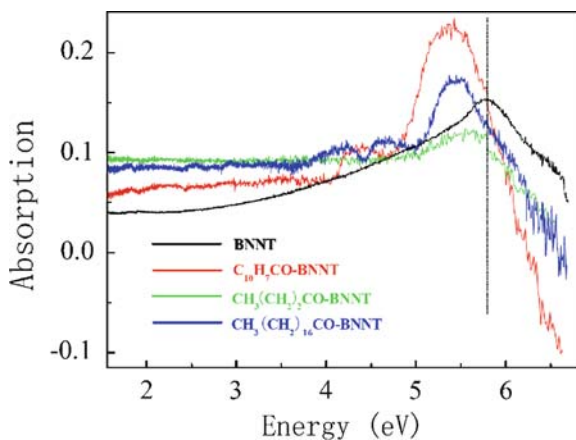**Fig. 11** Comparative UV–vis absorption spectra of pristine and functionalized BNNTs (courtesy of C. Y. Zhi; reprinted from [87]. © American Physical Society)

wall of BNNTs introduce additional absorption bands (Fig. 11), which reflect the modified band structure. These works have also indicated possible chemical modification of BNNTs for future chemical applications.

4.2.3 Functionalization for Molecular Biological Applications

In addition to chemical interactions, the BNNTs have been found to interact with biological molecules such as proteins or single-stranded deoxyribonucleic acid
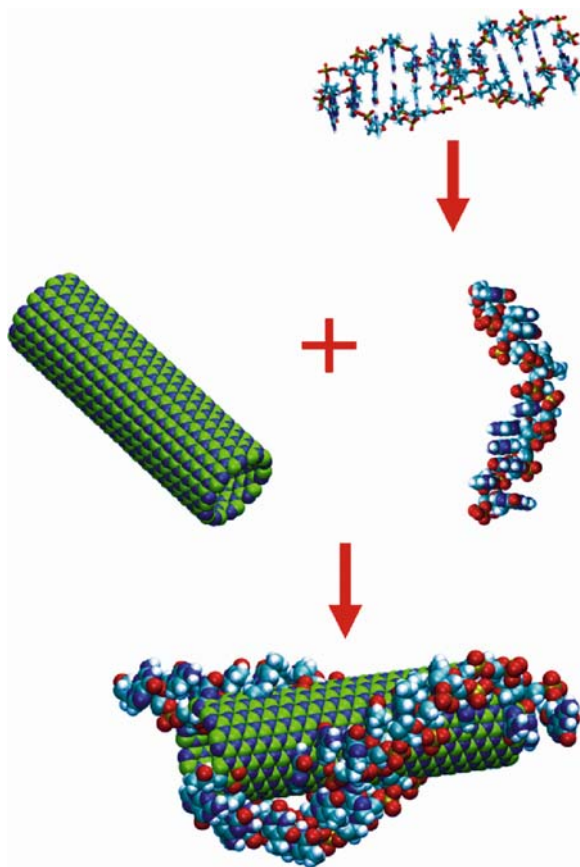
Fig. 12 The process of fabrication of a DNA–BNNT hybrid (courtesy of C. Y. Zhi; reprinted from [90]. © Wiley-VCH Verlag GmbH & Co. KGaA)

(ss-DNA) via π-stacking interactions with the side walls [89, 90]. Figure 12 illustrates a schematic of the wrapping of an ss-DNA molecule with a BNNT. Experimentally, this has been evidenced as shown by the TEM imaged in Fig. 13a, b. In addition, opened BNNTs can be filled with DNAs as shown in Fig. 13c. DNAs can also be removed by oxidation (annealing at 700°C for 30 min in air). As shown in Fig. 13d, DNAs are oxidized and fully removed to leave a clean BNNT surface. Functionalization of BNNTs with biomaterials opens a new way to incorporate biological molecules on BNNTs for biomedical and sensing applications. Of course, a lot of researches are necessary to be carried out to facilitate BNNTs in real-life applications.
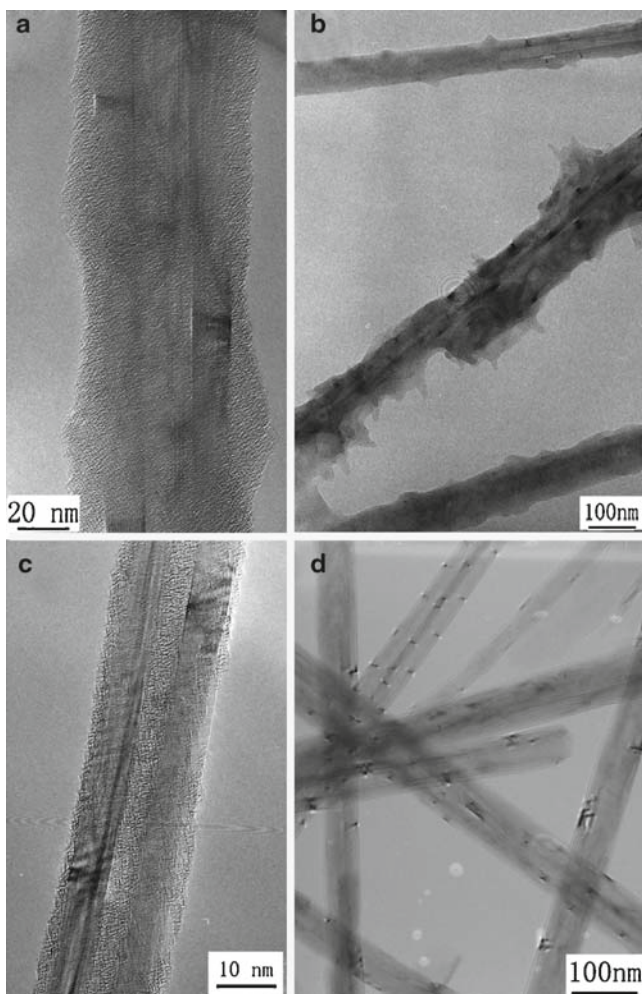
Fig. 13 (**a**) and (**b**) TEM images of BNNTs wrapped with DNA; (**c**) a DNA-filled BNNT (the *arrow* indicates the core area); (**d**) a DNA-BNNT sample annealed at 700°C for 30 min in air – the DNA is oxidized and fully removed to leave a clean BNNT surface (courtesy of C. Y. Zhi; reprinted from [90]. © Wiley-VCH Verlag GmbH & Co. KGaA)

5   Conclusions

In summary, significant breakthrough in high-yield synthesis of multiwalled BNNTs has been demonstrated by Golberg et al. and more recently by Yap et al. This has stimulated a series of investigations on chemical functionalization of

BNNTs. Promising results have been obtained on tuning the intrinsic properties of BNNTs. However, future research efforts are needed to demonstrate the performance of these functionalized BNNTs in mechanical, electronic, chemical, and biological applications. To date it is still challenging to control placement of BNNTs at desired locations of substrates for device integration. Another key issue will be doping of BNNTs to improve their electrical conductivity, which is required for most electronic devices. We point out here that effective CVD technique for the growth of single-wall BNNTs is still not available. Some of these issues have started to gain attention theoretically and experimentally as reviewed in Chaps. 3, 4, 5, and 7 of this book.

References

 1. A. Rubio, J. L. Corkill and M. L. Cohen, Phys. Rev. B 49 (1994) 5081.
 2. X. Blase, A. Rubio, S. G. Louie and M. L. Cohen, Europhys. Lett. 28 (1994) 335.
 3. N. G. Chopra, R. J. Luyken, K. Cherrey, V. H. Crespi, M. L. Cohen, S. G. Louie and A. Zettl, Science 269 (1995) 966.
 4. E. Hernandez, C. Goze, P. Bernier, and A. Rubio, Phys. Rev. Lett. 80 (1998) 4502.
 5. K. N. Kudin, G. E. Scuseria and B. I. Yakobson, Phys. Rev. B 64 (2001) 235406.
 6. A. P. Suryavanshi, M.-F. Yu, J. Wen, C. Tang and Y. Bando, Appl. Phys. Lett. 84 (2004) 2527.
 7. K. H. Khoo, M. S. C. Mazzoni and S. G. Louie, Phys. Rev. B 69 (2004) 201401R.
 8. C. W. Chen, M. H. Lee and S. J. Clark, Nanotechnology 15 (2004) 1837.
 9. M. Ishigami, J. D. Sau, S. Aloni, M. L. Cohen and A. Zettl, Phys. Rev. Lett. 94 (2005) 56804.
10. D. Golberg, Y. Bando, K. Kurashima and T. Sato, Scripta Mater. 44 (2001) 1561.
11. Y. Chen, J. Zou, S. J. Campbell, and G. L. Caer, Appl. Phys. Lett. 84 (2004) 2430.
12. C. Y. Zhi, Y. Bando, C. C. Tang, R. G. Xie, T. Sekiguchi and D. Golberg, J. Am. Chem. Soc. 127 (2005) 15996.
13. E. J. Mele and P. Kral, Phys. Rev. Lett. 88 (2002) 56803.
14. S. M. Nakhmanson, A. Calzolari, V. Meunier, J. Bernholc and M. B. Nardelli, Phys. Rev. B 67 (2003) 235406.
15. S. H. Jhi and Y. K. Kwon, Phys. Rev. B. 69 (2004) 245407.
16. X. Blase, J.-C. Charlier, A. De Vita, and R. Car, Appl. Phys. Lett. 70 (1997) 197.
17. J. Choi, Y.-H. Kim, K. J. Chang and D. Tománek, Phys. Rev. B 67 (2003) 125421.
18. M. Terrones, W. K. Hsu, H. Terrones, J. P. Zhang, S. Ramos, J. P. Hare, R. Castillo, K. Prassides, A. K. Cheetham, H. W. Kroto and D. R. M. Walton, Chem. Phys. Lett. 259 (1996) 568.
19. A. Loiseau, F. Willaime, N. Demoncy, G. Hug and H. Pascard, Phys. Rev. Lett. 76 (1996) 4737.
20. D. P. Yu, X. S. Sun, C. S. Lee, I. Bello, S. T. Lee, H. D. Gu, K. M. Leung, G. W. Zhu, Z. F. Dong and Z. Zhang, Appl. Phys. Lett. 72 (1988) 1966.
21. R. S. Lee, J. Gavillet, M. L. de le Chapelle, A. Loiseau, J.-L. Cochon, D. Pigache, J. Thibault and F. Willaime, Phys. Rev. B 64 (2001) 121405(R).
22. W. Q. Han, Y. Bando, K. Kurashima and T. Sato, Appl. Phys. Lett. 73 (1998) 3085.
23. Y. Chen, L. T. Chadderton, J. F. Gerald and J. S. Williams, Appl. Phys. Lett. 74 (1999) 2960.

24. O. R. Lourie, C. R. Jones, B. M. Bartlett, P. C. Gibbons, R. S. Ruoff and W. E. Buhro, Chem. Mater. 12 (2000) 1808.
25. C. C. Tang, X. X. Ding, X. T. Huang, Z. W. Gan, S. R. Qi, W. Liu and S. S. Fan, Chem. Phys. Lett. 456 (2002) 254.
26. C. C. Tang, Y. Bando, T. Sato, and K. Kurashima, Chem. Commun. (2002) 1290.
27. J. Wang, V. K. Kayastha, Y. K. Yap, Z. Y. Fan, J. G. Lu, Z. W. Pan, I. N. Ivanov, A. A. Puretzky, and D. B. Geohegan, Nano Lett. 5 (2005) 2528.
28. N. G. Chopra and A. Zettl, Solid State Commun. 105 (1998) 297.
29. E. Hernandez, C. Goze, P. Bernier and A. Rubio, Phys. Rev. Lett. 80 (1998) 4502.
30. D. Golberg, P. M. F. J. Costa, O. Lourie, M. Mitome, C. Tang, C. Y. Zhi, K. Kurashima, Y. Bando, Nano Lett. 7 (2007) 2146.
31. D. Sanchez-Portal and E. Hernandez, Phys. Rev. B 66 (2002) 235415.
32. L. Wirtz, A. Rubio, R. A. de la Concha and A. Loiseau, Phys. Rev. B 68 (2003) 045425.
33. V. N. Popov, Phys. Rev. B 67 (2003) 85408.
34. Y. Xiao, X. H. Yan, J. X. Cao, J. W. Ding, Y. L. Mao and J. Xiang, Phys. Rev. B 69 (2004) 205415.
35. C. C. Tang, Y. Bando, C. H. Liu, S. S. Fan, J. Zhang, X. X. Ding and D. Golberg, J. Phys. Chem B 110 (2006) 10354.
36. M. Radosavljevic, J. Appenzeller, V. Derycke, R. Martel, Ph. Avouris, A. Loiseau, J.-L. Cochon and D. Pigache, Appl. Phys. Lett. 82 (2003) 4131.
37. Y. Miyamoto, A. Rubio, M. L. Cohen and S. G. Louie, Phys. Rev. B 50 (1994) 4976.
38. Y.-H. Kim, K. J. Chang and S. G. Louie, Phys. Rev. B 63 (2001) 205408.
39. X. Bai, D. Golberg, Y. Bando, C. Zhi, C. Tang, M. Mitome and K. Kurashima, Nano Lett. 7 (1997) 632.
40. J. Cummings and A. Zettle, Solid State Commun. 129 (2004) 661.
41. M. F. Ng and R. Q. Zhang, Phys. Rev. B 69 (2004) 115417.
42. P. Kral, E. J. Mele and D. Tomanek, Phys. Rev. Lett. 85 (2000) 1512.
43. J. Kongsted, A. Osted, L. Jensen, P.-O. Astrand and K. V. Mikkelsen, J. Phys. Chem. B 105 (2001) 10243.
44. D. Golberg, Y. Bando, M. Eremets, K. Takemura, K. Kurashima, T. Tamiya, H. Yusa, Appl. Phys. Lett. 69 (1996) 2045.
45. Y. Chen, M. Conway, J. S. Williams and J. Zou, J. Mater. Res. 17 (2002) 1896.
46. M. J. Kim, S. Chatterjee, S. M. Kim, E. A. Stach, M. G. Bradley, M. J. Pender, L. G. Sneddon and B. Maruyama, Nano Lett. 8 (2008) 3298.
47. K. P. Loh, M. Lin, M. Yeadon, C. Boothroyd and Z. Hu, Chem. Phys. Lett. 387 (2004) 40.
48. E. Bengu and L. D. Marks, Phys. Rev. Lett. 86 (2001) 2385.
49. Y. Shimizu, Y. Moriyoshi, H. Tanaka and S. Komatsu, Appl. Phys. Lett. 75 (1999) 929.
50. C. H. Lee, J. Wang, V. K. Kayastha, J. Y. Haung and Y. K. Yap, Nanotechnology 19 (2008) 455605.
51. S. L. Mensah, A. Prasad, J. Wang and Y. K. Yap, J. Nanosci. Nanotechnol. 8 (2008) 233.
52. J. P. Moscatello, J. Wang, B. Ulmen, S. L. Mensah, M. Xie, S. Wu, A. Pandey, C. H. Lee, A. Prasad, V. K. Kayasha and Y. K. Yap, in *Special Issue on Nanosensors for Defense and Security*, IEEE Sensor Journal 8 (2008) 922.
53. S. L. Mensah, V. K. Kayastha, I. N. Ivanov, D. B. Geohegan and Y. K. Yap, Appl. Phys. Letts. 90 (2007) 113108.
54. V. K. Kayastha, S. Wu, J. Moscatello and Y. K. Yap, J. Phys. Chem. C (Letter) 111 (2007) 10158.
55. S. L. Mensah, V. K. Kayastha and Y. K. Yap, J. Phys. Chem. C (Letter) 111 (2007) 16092.
56. V. K. Kayastha, Y. K. Yap, Z. Pan, I. N. Ivanov, A. A. Puretzky and D. B. Geohegan, Appl. Phys. Lett. 86 (2005) 253105.
57. V. Kayastha, Y. K. Yap, S. Dimovski and Y. Gogotsi, Appl. Phys. Lett. 85 (2004) 3265.
58. Y. K. Yap, T. Aoyama, S. Kida, Y. Mori and T. Sasaki, Diamond Relat. Mater. 8 (1999) 382.
59. J. Wang and Y. K. Yap, Diamond Relat. Mater. 15 (2006) 444.
60. P. Jaffrennou, J. Barjon, J. S. Lauret, A. Maguer, D. Golberg, B. Attal-Trétout, F. Ducastelle and A. Loiseau, Phys. Status Solidi B 244 (2007) 4147.

61. R. Arenal, O. Stephan, M. Kociak, D. Taverna, A. Loiseau and C. Colliex, Phys. Rev. Lett. 95 (2005) 127601.
62. Y. Kubota, K. Watanabe, O. Tsuda and T. Taniguchi, Science 317 (2007) 932.
63. X. J. Wu, J. L. Yang and X. C. Zeng, J. Chem. Phys. 125 (2006) 44704.
64. C. Zandonella, Nature 410 (2001) 734.
65. S. H. Jhi, Phys. Rev. B 74 (2006) 155424.
66. R. J. Baierle, P. Piquini, T. M. Schmid and A. Fazzio, J. Phys. Chem. B 110 (2006) 21184.
67. R. Z. Ma, Y. Bando, H. W. Zhu, T. Sato, C. L. Xu and D. H. Wu, J. Am. Chem. Soc. 124 (2002) 7672.
68. J. Chen, M. A. Hamon, H. Hui, Y. Chen, A. M. Rao, P. C. Eklund and R. C. Haddon, Science 282 (1998) 95.
69. A. Star, J. F. Stoddart, D. Steuerman, M. Diehl, A. Boukai, E. W. Wong, X. Yang, S. W. Chung, H. Choi and J. R. Heath, Angew. Chem. Int. Ed. 40 (2001) 1721.
70. J. Chen, H. Liu, W. A. Weimer, M. D. Halls, D. H. Waldeck and G. C. Walker, J. Am. Chem. Soc. 124 (2002) 9034.
71. V. Georgakilas, K. Kordatos, M. Proto, D. M. Guldi, M. Holzinger and A. Hirsch, J. Am. Chem. Soc. 124 (2002) 760.
72. A. Bianco and M. Prato, Adv. Mater. 15 (2003) 1765.
73. K. Jiang, Q. Li and S. Fan, Nature 419 (2002) 801.
74. A. A. Mamedov, N. A. Kotov, M. Prato, D. M. Guldi, J. P. Wicksted and A. Hirsch, Nat. Mater. 1 (2002) 190.
75. B. R. Azamian, J. J. Davis, K. S. Coleman, C. B. Bagshaw and M. L. Green, J. Am. Chem. Soc. 124 (2002) 12664.
76. A. B. Dalton, S. Collins, E. Muñoz, J. M. Razal, V. H. Ebron, J. P. Ferraris, J. N. Coleman, B. G. Kim and R. H. Baughman, Nature 423 (2003) 703.
77. Y. Kang and T. A. Taton, J. Am. Chem. Soc. 125 (2003) 5650.
78. K. A. Williams, P. T. M. Veenhuizen, B. G. de la Torre, R. Eritjia and C. Dekker, Nature 420 (2002) 761.
79. H. Xin and A. T. Woolley, J. Am. Chem. Soc. 125 (2003) 8710.
80. J. J. Gooding, R. Wibowo, J. Liu, W. Yang, D. Losic, S. Orbons, F. J. Mearns, J. G. Shapter and D. B. Hibbert, J. Am. Chem. Soc. 125 (2003) 9006.
81. R. J. Chen, S. Bangsaruntip, K. A. Drouvalakis, N. W. S. Kam, M. Shim, Y. Li, W. Kim, P. J. Utz, and H. Dai, Proc. Natl. Acad. Sci. USA 100 (2003) 4984.
82. W. Q. Han and A. Zettl, J. Am. Chem. Soc. 125 (2003) 2062.
83. C. Y. Zhi, Y. Bando, C. Tang and D. Golberg, J. Phys. Chem. B 110 (2006) 8548.
84. C. Y. Zhi, Y. Bando, C. Tang and D. Golberg, Solid State Commun. 136 (2005) 67.
85. S. Y. Xie, W. Wang, K. A. S. Fernando, X. Wang, Y. Lin and Y. P. Sun, Chem. Commun. (2005) 3670.
86. C. Y. Zhi, Y. Bando, C. Tang and D. Golberg, J. Phys. Chem. B 110 (2006) 1525.
87. C. Y. Zhi, Y. Bando, C. Tang and D. Golberg, Phys. Rev. B 74 (2006) 153413.
88. C. Y. Zhi, Y. Bando, C. Tang, S. Honda, K. Sato, H. Kuwahara and D. Golberg, Angew. Chem. Int. Ed. 44 (2005) 7932.
89. C. Y. Zhi, Y. Bando, C. Tang and D. Golberg, J. Am. Chem. Soc. 127 (2005) 17144.
90. C. Y. Zhi, Y. Bando, W. Wang, C. Tang, H. Kuwahara and D. Golberg, Chem. Asaian J. 2 (2007) 1581.